

# Nonlinear Magnon Spin Nernst Effect in Antiferromagnets and Strain-tunable Pure Spin Current

Hiroki Kondo and Yutaka Akagi

*Department of Physics, Graduate School of Science,  
The University of Tokyo, 7-3-1 Hongo, Tokyo 113-0033, Japan\**

In this Letter, we study the spin Nernst effect of magnons in the nonlinear response regime. We derive the formula for the nonlinear magnon spin Nernst current by solving the Boltzmann equation and find out that it is described by an extended Berry curvature dipole of magnons. The nonlinear magnon spin Nernst effect is expected to occur in various Néel antiferromagnetic materials even without the Dzyaloshinskii-Moriya interaction. In particular, the nonlinear spin Nernst current in the honeycomb and diamond lattice antiferromagnets can be controlled by strain/pressure.

*Introduction.*—The Berry phase and curvature play an essential role in modern condensed matter physics; e.g., they are responsible for polarization, orbital magnetism, and various types of Hall effects [1]. In particular, it is well-known that in the linear response regime, the Hall effect [2, 3] and the spin Hall effect [4–7] are described by the integral of Berry curvature (BC). Recently, transport phenomena have been further explored by taking into account the nonlinear response contributions. A remarkable study is the nonlinear Hall effect [8]. Even in materials with time-reversal symmetry, transverse electric current can emerge as the second-order response to an electric field [8–24]. It originates from a dipole moment of the BC in the crystal momentum space, named the Berry curvature dipole (BCD) [8], which appears in the systems breaking inversion and rotational symmetries.

Even in bosonic systems, it has also been clarified that the Berry phase and curvature are relevant to their physics, by the theoretical studies and experimental observation of the thermal Hall effect of magnons [25–43], which are bosonic quasiparticles of spin waves. In association with the Berry curvature in magnets, various topological magnon systems have been proposed; e.g., magnonic analogs of spin Hall insulators [44–47], three-dimensional topological insulators [48], topological crystalline insulators [49], and Dirac and Weyl semimetals [50–58], which provide a venue for the unprecedented transport phenomena in insulating magnetic materials. Among them, it is worthy to note that the magnon spin Nernst effect (SNE) [44–46, 59] has been observed in antiferromagnets (AFMs) [60], which makes it possible to generate the spin current of magnons with long coherence and promise their potential applications in spintronics [61, 62].

Despite a number of studies on magnon systems, representative transport phenomena, e.g., thermal Hall effect and SNE of magnons, have been considered mostly in the magnets with the Dzyaloshinskii-Moriya interaction (DMI) or noncollinear spin configurations, which give rise to complex hopping matrix elements in the magnon Hamiltonian. This is because their manifestation as a lin-

ear response requires the integration of the magnon BC over the whole Brillouin zone to be nonzero. In order to relax the restrictions on such magnon transport phenomena, we should explore the region beyond the linear response regime as one option. As in the case of electronic systems, by investigating the magnon nonlinear response, nontrivial transport phenomena are expected to be discovered in magnets even without the DMI or noncollinear spin configuration. So far, the nonlinear Hall effect [63], spin Seebeck effect [64], and optical response [65, 66] of magnons have been proposed. However, research on the nonlinear response of magnons is just beginning to emerge.

In this Letter, we study the magnon second-order response to the temperature gradient by solving the Boltzmann equation and show that the nonlinear magnon spin Nernst current can be described by an extended BCD. As shown later, the extended BCD is easily found in collinear Néel AFMs without the DMI, whereas the manifestation of BC, which is responsible for the linear magnon SNE and thermal Hall effect, requires the DMI or noncollinear spin configuration. Therefore, it is expected that various Néel AFMs even without the DMI can exhibit the nonlinear SNE of magnons, while the magnon thermal Hall effect, as well as the linear magnon SNE, is absent. As a demonstration, we apply the obtained formula to the strained honeycomb lattice AFM without the DMI. A remarkable result is that the direction of the spin current can be controlled by tuning the strain. We also investigate several other models for Néel AFMs and find the presence of (extended) BCD, which results in nonlinear magnon SNE.

*Expression of nonlinear spin Nernst current.*—First, we derive the formula for the magnon spin Nernst current up to the second-order response to the temperature gradient. We begin with the expression of the transverse magnon current in Ref. [26]:

$$J_y = -\frac{1}{\hbar V} \sum_{n, \mathbf{k}} \Omega_n(\mathbf{k}) \int_0^\infty d\epsilon \frac{\partial}{\partial x} \rho(E_n(\mathbf{k}) + \epsilon, T(x)), \quad (1)$$

where  $E_n(\mathbf{k})$  and  $\Omega_n(\mathbf{k})$  are the energy eigenvalue and BC of the  $n$ th band with the wave vector  $\mathbf{k}$ , respectively. Here,  $\rho(E, T(x))$  is a distribution function for magnons with the energy  $E$  under the temperature  $T(x)$ . We as-

\* kondo-hiroki290@g.ecc.u-tokyo.ac.jp

sume that the temperature gradient is applied in the  $x$ -direction as  $T(x) = T_0 - x\nabla T$ . The parameters  $T_0$  and  $\nabla T$  denote the average temperature and the temperature gradient, respectively.

Next, we consider the Boltzmann equation to derive the formula for the nonlinear response from Eq. (1). Hereafter, we assume the steady-state and the system without external field, then the Boltzmann equation in the relaxation time approximation [67–69] is written as follows [70]:

$$\begin{aligned} \dot{x} \frac{\partial}{\partial x} \rho(E_n(\mathbf{k}) + \epsilon, T(x)) \\ = - \frac{\rho(E_n(\mathbf{k}) + \epsilon, T(x)) - \rho_0(E_n(\mathbf{k}) + \epsilon, T(x))}{\tau}. \end{aligned} \quad (2)$$

where  $\tau$  and  $\rho_0(E, T(x))$  are the relaxation time of magnons and the equilibrium distribution function  $\rho_0(E, T(x)) = [e^{E/T(x)} - 1]^{-1}$ , respectively. Since the position dependence is included only in the temperature  $T(x) = T_0 - x\nabla T$ , the  $x$ -derivative can be replaced as  $\partial/\partial x \rightarrow -\nabla T \partial/\partial T$ . It implies that the first- and second-order differentiations of  $\rho_0(E_n(\mathbf{k}) + \epsilon, T(x))$  in  $x$  give the first- and second-order responses to the temperature gradient  $\nabla T$ , respectively. In the Supplemental Materials [70], we solve Eq. (2) up to first-order in  $\nabla T$  which corresponds to the second-order responses since another  $\nabla T$  factor comes from the  $x$ -derivative in Eq. (1).

By substituting the obtained nonequilibrium distribution function  $\rho(E_n(\mathbf{k}) + \epsilon, T(x))$  to Eq. (1), we derive the formula for the transverse magnon current up to the second-order in  $\nabla T$ . It can be written as follows [70]:

$$\begin{aligned} J_y = \frac{\nabla T}{\hbar V} \sum_n \int_{\text{BZ}} d^2 k c_1(\rho_0(E_n(\mathbf{k}), T_0)) \Omega_n(\mathbf{k}) \\ + \frac{\tau(\nabla T)^2}{\hbar^2 V T_0} \sum_n \int_{\text{BZ}} d^2 k c_1(\rho_0(E_n(\mathbf{k}), T_0)) \frac{\partial}{\partial k_x} (E_n(\mathbf{k}) \Omega_n(\mathbf{k})) \\ + O((\nabla T)^3), \end{aligned} \quad (3)$$

where the function  $c_1(\rho_0)$  is defined as  $c_1(\rho_0) := (1 + \rho_0) \ln(1 + \rho_0) - \rho_0 \ln \rho_0$ . The first term on the right-hand side has been obtained in Ref. [26]. The second term describes the nonlinear response in magnon systems.

In the following, we focus on the magnons in Néel AFMs, assuming that the spins are aligned in the  $z$ -direction. In terms of magnons, the systems have  $\mathcal{PT}$ -symmetry due to the perfect staggered magnetization; i.e., the magnon Hamiltonian  $H(\mathbf{k})$  satisfies the following equation

$$(\mathcal{PT})^{-1} \Sigma_z H(\mathbf{k}) \mathcal{PT} = \Sigma_z H(\mathbf{k}), \quad (4)$$

where  $\mathcal{P}$  and  $\mathcal{T}$  are parity and time-reversal operators, respectively. The matrix  $\Sigma_z$  is defined as  $\Sigma_z = \sigma_z \otimes 1_N$ , where  $\sigma_i$  ( $i = x, y, z$ ),  $N$ , and  $1_N$  are the  $i$ -component of the Pauli matrix, the number of the sublattices in the unit cell, and  $N$ -dimensional identity matrix, respectively. We note that  $\Sigma_z H(\mathbf{k})$  in Eq. (4) is the effective Hamiltonian for magnons in the AFMs, whose form gives

rise to non-Hermiticity [71]. As long as the systems conserve the total spin in the  $z$ -direction  $S^z$ , we always have two degenerate magnon states related by  $\mathcal{PT}$ -operator.

We here write the eigenvectors and BC of magnons with the up (down) spin dipole moment as  $\psi_{n,\uparrow(\downarrow)}(\mathbf{k})$  and  $\Omega_{n,\uparrow(\downarrow)}(\mathbf{k})$ , respectively. Since each magnon excitation carries the spin angular momentum  $\pm \hbar$  in systems with conservation of the total spin along the  $z$ -direction, the magnon spin Nernst current  $J_y^S = \hbar(J_{y,\uparrow} - J_{y,\downarrow})$  can be written as follows:

$$\begin{aligned} J_y^S = \frac{\nabla T}{V} \sum_n \int_{\text{BZ}} d^2 k c_1(\rho_0(E_n(\mathbf{k}), T_0)) (\Omega_{n,\uparrow}(\mathbf{k}) - \Omega_{n,\downarrow}(\mathbf{k})) \\ + \frac{\tau(\nabla T)^2}{\hbar V T_0} \sum_n \int_{\text{BZ}} d^2 k c_1(\rho_0(E_n(\mathbf{k}), T_0)) \\ \times \frac{\partial}{\partial k_x} [E_n(\mathbf{k}) (\Omega_{n,\uparrow}(\mathbf{k}) - \Omega_{n,\downarrow}(\mathbf{k}))] \\ + O((\nabla T)^3), \end{aligned} \quad (5)$$

where the magnon BC is defined as  $\Omega_{n,\uparrow(\downarrow)}(\mathbf{k}) = -2\text{Im}[(\partial_{k_x} \psi_{\uparrow(\downarrow)}(\mathbf{k}))^\dagger \Sigma_z (\partial_{k_y} \psi_{\uparrow(\downarrow)}(\mathbf{k}))]$ , slightly different from BC in fermionic systems due to the non-Hermiticity in the magnon (bosonic) Bogoliubov-de Gennes systems. We remark that the spin Nernst current as a second-order response is described in terms of not BCD  $D_{n,\uparrow(\downarrow)}^x(\mathbf{k}) := (\partial/\partial k_x)(\Omega_{n,\uparrow(\downarrow)}(\mathbf{k}))$ , but the BCD-like quantity:  $(\partial/\partial k_x)[E_n(\mathbf{k})(\Omega_{n,\uparrow}(\mathbf{k}) - \Omega_{n,\downarrow}(\mathbf{k}))]$ , which we call extended BCD. We also note that the magnon thermal Hall current defined in Ref. [26] is absent because  $\Omega_{n,\uparrow}(\mathbf{k}) = -\Omega_{n,\downarrow}(\mathbf{k})$  holds due to  $\mathcal{PT}$ -symmetry.

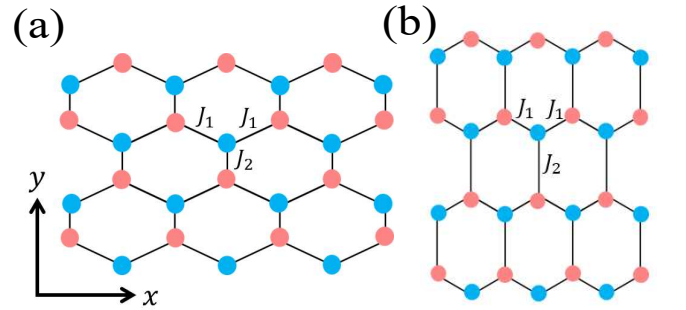


FIG. 1: Honeycomb lattice AFMs extended along the (a)  $x$ -direction and (b)  $y$ -direction, which correspond to (a)  $J_1 < J_2$  and (b)  $J_1 > J_2$ . Red and blue circles denote spins pointing upward and downward, respectively.

*Model.*— As the first model exhibiting the nonlinear magnon SNE, we consider a honeycomb lattice AFM with strain, which is illustrated in Fig. 1. The Hamiltonian of the AFM is written as follows:

$$\mathcal{H} = J_1 \sum_{\langle ij \rangle_1} \mathbf{S}_i \cdot \mathbf{S}_j + J_2 \sum_{\langle ij \rangle_2} \mathbf{S}_i \cdot \mathbf{S}_j - \kappa \sum_i (S_i^z)^2, \quad (6)$$

where  $\mathbf{S}_i = (S_i^x, S_i^y, S_i^z)$  denotes the spin at site  $i$ . Here,  $\langle ij \rangle_2$  and  $\langle ij \rangle_1$  are the nearest-neighbor vertical bonds and the other ones shown in Fig. 1, respectively. The

third term is an easy-axis anisotropy in the  $z$ -direction. By applying Holstein-Primakoff and Fourier transformations, we can obtain the magnon Hamiltonian as follows:

$$\mathcal{H} = \frac{1}{2} \sum_{\mathbf{k}} \psi^\dagger(\mathbf{k}) H(\mathbf{k}) \psi(\mathbf{k}),$$

$$H(\mathbf{k}) = \begin{pmatrix} d & 0 & 0 & \gamma(\mathbf{k}) \\ 0 & d & \gamma^*(\mathbf{k}) & 0 \\ 0 & \gamma(\mathbf{k}) & d & 0 \\ \gamma^*(\mathbf{k}) & 0 & 0 & d \end{pmatrix},$$

$$\psi^\dagger(\mathbf{k}) = [b_\uparrow^\dagger(\mathbf{k}), b_\downarrow^\dagger(\mathbf{k}), b_\uparrow(-\mathbf{k}), b_\downarrow(-\mathbf{k})]. \quad (7)$$

Here,  $d$  and  $\gamma(\mathbf{k})$  are defined as  $d = 2J_1S + J_2S + 2\kappa S$  and  $\gamma(\mathbf{k}) = 2J_1S e^{ik_y/2\sqrt{3}} \cos(k_x/2) + J_2S e^{-ik_y/\sqrt{3}}$ , respectively, where  $S$  is the spin magnitude. The operator  $b_{\uparrow(\downarrow)}(\mathbf{k})$  is the annihilation operator of magnons with the spin dipole moments upward (downward), i.e., magnons from spins pointing downward (upward). The parity and time-reversal operators of this model are defined as  $\mathcal{P} = 1_2 \otimes \sigma_x$  and  $\mathcal{T} = K$ , respectively. Here,  $K$  is the complex conjugation operator. One can easily confirm that the Hamiltonian  $H(\mathbf{k})$  satisfies the  $\mathcal{PT}$ -symmetry in Eq. (4).

*Nonlinear magnon spin Nernst effect.*— Figure 3 shows the band structure, BC, and BCD of magnons with up spin dipole moment in the strained honeycomb AFM. Those of magnons with down spin dipole moment are determined by  $E_\downarrow(\mathbf{k}) = E_\uparrow(\mathbf{k})$ ,  $\Omega_\downarrow(\mathbf{k}) = -\Omega_\uparrow(\mathbf{k})$ , and  $D_\downarrow^x(\mathbf{k}) = -D_\uparrow^x(\mathbf{k})$ , respectively. As shown in Figs. 3(c) and (d), BC of magnons is antisymmetric about  $\Gamma$  point. This property corresponds to finite BCD [see Figs. 3(e) and (f)] which appears due to breaking inversion and rotational symmetries. We note that BCD itself is plotted hereafter, instead of the extended BCD, since they contribute to nonlinear SNE of magnons similarly.

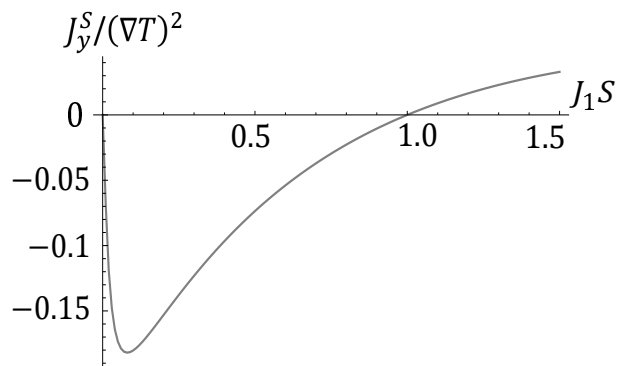


FIG. 2: Coefficient of the nonlinear magnon SNE in the honeycomb AFM as a function of the coupling constant  $J_1$ . The coupling constant  $J_2$ , the easy-axis anisotropy, and the average temperature are taken to be  $J_2S = 1.0$ , and  $\kappa S = 0.01$ , and  $T_0 = 0.1$ , respectively. Here, we take the factor  $\tau/(\hbar VT_0)$  to be unity.

Figure 2 shows the coefficient of the nonlinear magnon SNE given by Eq. (5) in the honeycomb AFM as a func-

tion of the coupling constant  $J_1$ . As expected, the coefficient becomes zero for  $J_1 = 0$  and  $J_1 = J_2$  (corresponding to the system with the three-fold rotational symmetry restored). It is noteworthy that spin current flows in the  $+y$ -direction and the  $-y$ -direction in the cases of  $J_1 < J_2$  and  $J_1 > J_2$ , respectively. It implies that the direction of the spin current can be controlled by tuning the strain.

We also note that magnon SNE in the linear response regime is absent due to the system without the DMI [72]. In addition, the system does not exhibit the magnon thermal Hall effect due to  $\Omega_\downarrow(\mathbf{k}) = -\Omega_\uparrow(\mathbf{k})$  and  $E_\downarrow(\mathbf{k}) = E_\uparrow(\mathbf{k})$ .

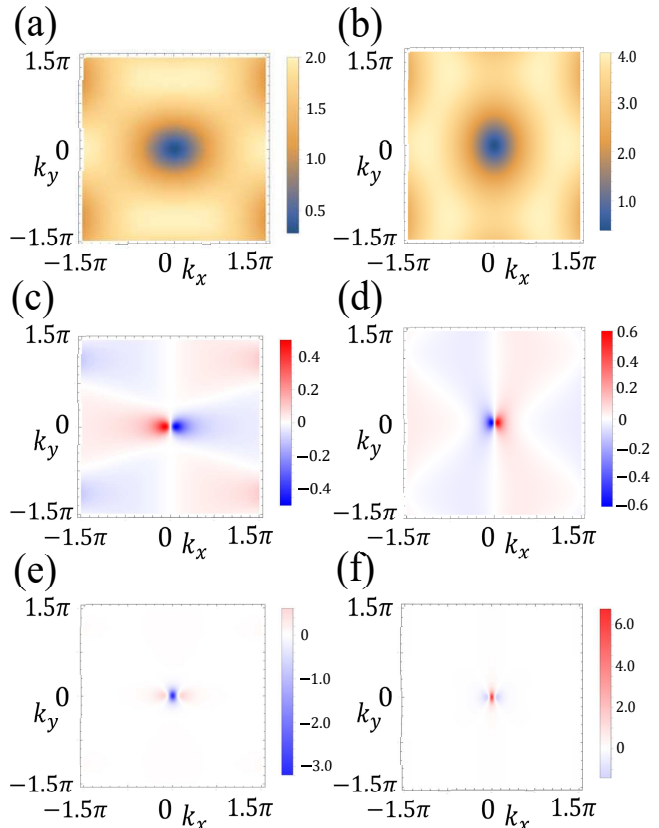


FIG. 3: (a), (b) Band structure  $E_\uparrow(\mathbf{k})$ , (c), (d) BC  $\Omega_\uparrow(\mathbf{k})$ , and (e), (f) BCD  $D_\uparrow^x(\mathbf{k})$  of magnons with the up spin dipole moment in the strained honeycomb lattice antiferromagnet. The parameters in (a), (c), and (e) are chosen to be  $J_1S = 0.5$ ,  $J_2S = 1.0$ , and  $\kappa S = 0.01$ , which is the case described in Fig. 1(a). In (b), (d), and (f), we take the parameters to be  $J_1S = 1.5$ ,  $J_2S = 1.0$ , and  $\kappa S = 0.01$ , corresponding to Fig. 1(b).

Here, let us discuss the order of the nonlinear magnon SNE, by comparing it to the linear one observed in the honeycomb antiferromagnet  $\text{MnPS}_3$  [60] with the DMI  $D$ . Through the inverse spin Hall effect, the linear SNE was observed with an electric voltage  $V_L \sim 1 \mu\text{V}$  under  $T_0 \sim 20 \text{ K}$  and  $\nabla T \sim 10^{-6} \text{ K} \cdot \text{nm}^{-1}$  [60]. As discussed in the Supplemental Materials [70], the theoretical value of linear spin Nernst current  $J_L^S$ , which corresponds to the first term in Eq. (5), is evaluated as  $J_L^S \sim (\nabla T/V) \times 10^{-1}$

for  $J_1 = J_2 = 1.54$  meV,  $D = 0.36$  meV,  $\kappa S = 0.0086$  meV, and  $S = 5/2$  taken from Refs. [59, 73] for MnPS<sub>3</sub>. On the other hand, the spin current due to nonlinear SNE is estimated to be  $J_{NL}^S \sim (\tau(\nabla T)^2/\hbar V) \times 10^{-1}$  if the parameters  $J_1$  and  $D$  are changed to 2.0 meV and zero from those in MnPS<sub>3</sub>, respectively. Therefore, in the absence of the DMI, the order of the voltage for nonlinear SNE is  $V_{NL} \sim V_L \times (J_{NL}^S/J_L^S) \sim 10^{n+6} \mu\text{V}$ , when the lifetime of magnons is  $\tau \sim 10^n$  s. In experiments, the minimum voltage detectable is roughly in the order of  $10^{-3} \mu\text{V}$  [74]. Thus, we can detect the nonlinear SNE for  $\tau \sim 1$  ns, where in model (6), the corresponding mean free path is  $l \sim 1 \mu\text{m}$  achievable in magnets.

*Berry curvature dipole in various antiferromagnets—*  
In this part, we showcase the magnon BCD in several AFMs; square lattice AFMs with bond dependences and diamond lattice AFM under pressure [See Fig. 4]. The forms of the Hamiltonians in these three cases are the same as Eq. (6). Figure 4 shows which nearest neighbor bonds correspond to  $\langle ij \rangle_1$  and  $\langle ij \rangle_2$  in the Hamiltonians. The explicit expressions of the magnon Hamiltonian for these systems are detailed in the Supplemental Materials [70, 75].

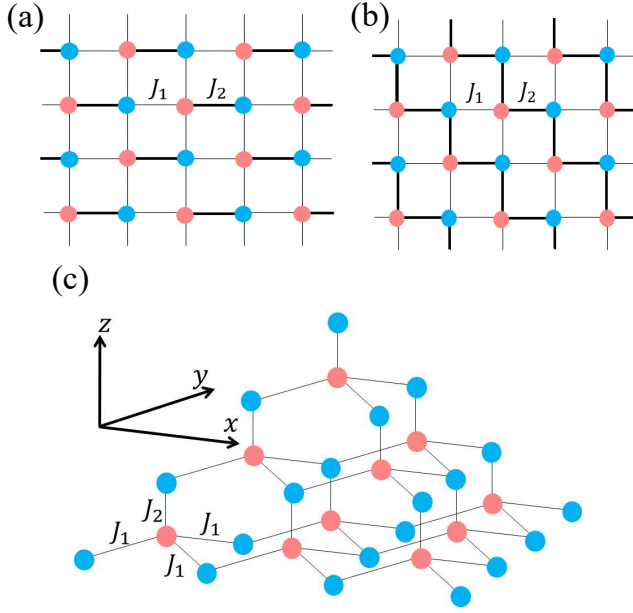


FIG. 4: Square lattice AFMs with (a) staggered- and (b) zigzag-bond dependences. The nearest neighbor bonds  $\langle ij \rangle_1$  and  $\langle ij \rangle_2$  in Eq. (6) correspond to the ones denoted by the thin and thick lines, respectively. (c) Diamond lattice AFM under pressure from the  $z$ -direction. The bonds  $\langle ij \rangle_2$  and  $\langle ij \rangle_1$  in Eq. (6) correspond to the vertical and the other three ones, respectively.

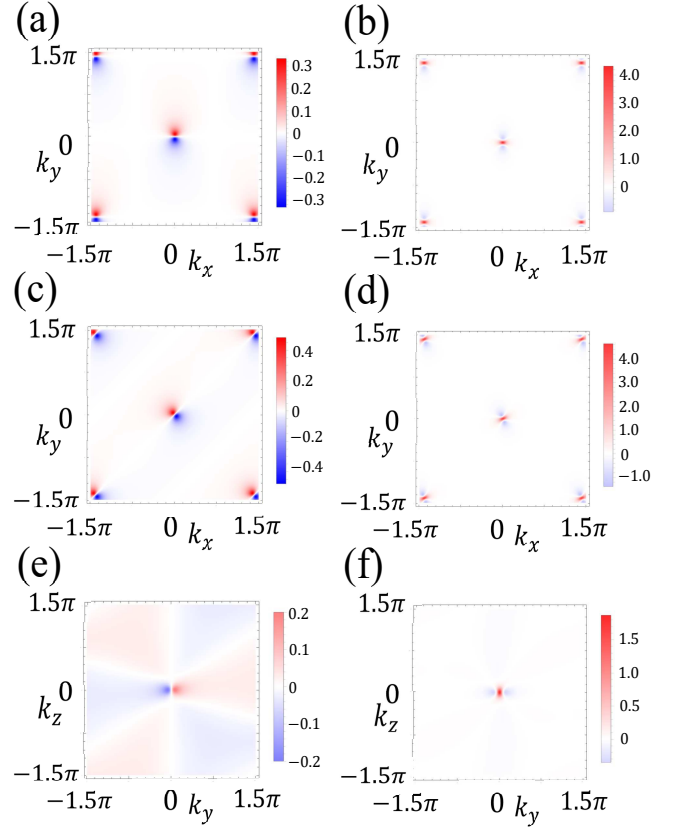


FIG. 5: (a),(c) BC  $\Omega_{\uparrow}(\mathbf{k})$  and (b),(d) BCD  $D_{\uparrow}^y(\mathbf{k}) = \partial_{k_y}\Omega_{\uparrow}(\mathbf{k})$  of magnons with the up spin dipole moment in the square lattice AFM. (a) and (b) ((c) and (d)) are results for the staggered-bond (zigzag-bond) dependence described in Fig. 4(a) (Fig. 4(b)). Figures (e) and (f) show the  $x$ -component of BC  $\Omega_{\uparrow}^x(0, k_y, k_z)$  and BCD  $D_{\uparrow}^{xy}(0, k_y, k_z)$  of magnons in the diamond lattice AFM under pressure, respectively. The parameters in these systems are chosen to be  $J_1 S = 1.0$ ,  $J_2 S = 1.2$ , and  $\kappa S = 0.01$ .

Figure 5 shows BC and BCD of magnons in these systems. For the diamond lattice AFM, we plot the  $x$ -component of BC and BCD defined as  $\Omega_{\uparrow}^x(\mathbf{k}) = 2\text{Im}[(\partial_{k_y}\psi_{\uparrow}(\mathbf{k}))^\dagger \Sigma_z (\partial_{k_z}\psi_{\uparrow}(\mathbf{k}))]$  and  $D_{\uparrow}^{xy}(\mathbf{k}) = \partial_{k_y}\Omega_{\uparrow}^x(\mathbf{k})$  in the  $k_x = 0$  plane, respectively. They are relevant for nonlinear magnon SNE in three dimensions [see Supplemental Materials [70] for detailed expression]. As in the case of honeycomb lattice AFM, the energy eigenvalue, BC, and BCD of magnons with down spin dipole moment in the square (diamond) lattice AFM are determined by  $E_{\downarrow}(\mathbf{k}) = E_{\uparrow}(\mathbf{k})$ ,  $\Omega_{\downarrow}(\mathbf{k}) = -\Omega_{\uparrow}(\mathbf{k})$  ( $\Omega_{\downarrow}^x(\mathbf{k}) = -\Omega_{\uparrow}^x(\mathbf{k})$ ), and  $D_{\downarrow}(\mathbf{k}) = -D_{\uparrow}(\mathbf{k})$  ( $D_{\downarrow}^{xy}(\mathbf{k}) = -D_{\uparrow}^{xy}(\mathbf{k})$ ), respectively. As shown in Fig. 5, BCD appears around  $\Gamma$  point, which contributes to the nonlinear SNE. In fact, the AFMs considered here can exhibit the nonlinear SNE of magnons in all cases [see Fig. S3 in Supplemental Materials [70] for details]. We here emphasize that the pressure-tunable spin current can be expected in the diamond lattice AFM as well, while the bond dependences on a square lattice are hard to realize by mechanical ways.

*Summary*— In this Letter, we have derived the formula for the magnon spin Nernst current as a second-order response and found that it is characterized by the extended BCD. We then have applied the obtained formula to the strained honeycomb lattice AFMs and found out that the direction of spin current can be controlled by tuning the strain. We have also calculated the magnon BCD and confirmed that the nonlinear magnon SNE appears in the square lattice AFMs with bond dependences and the diamond lattice AFM under pressure. Even without the DMI, the nonlinear magnon SNE is expected to be brought about in various Néel AFMs when the inversion and rotational symmetries are broken by such as strain/pressure [76].

Our study reveals that the pure spin current can be generated in various Néel AFMs. Owing to the simple setup, we can find a number of candidate antiferromagnetic materials exhibiting nonlinear magnon SNE; e.g., AFMs on a honeycomb lattice [77–83], square lattice with

zigzag bond dependence [84], and diamond lattice [85–87]. We here emphasize that our proposal for the nonlinear magnon SNE provides one of a few possible ways to generate the spin current in materials composed of light elements such as organic materials [88, 89] where the DMI is negligible. Since such organic materials [79, 87] are easily deformed mechanically, we expect to have a controllable pure spin current by strain or pressure, which expands the possibilities of applications in spintronics.

*Acknowledgements*.— We acknowledge valuable discussions with Hosho Katsura. We also thank Masahiro Sato, Hitoshi Seo, Tokuro Shimokawa for their fruitful comments. This work was supported by JSPS KAKENHI Grants No. JP17K14352, JP20K14411, JP20J12861, and JSPS Grant-in-Aid for Scientific Research on Innovative Areas “Quantum Liquid Crystals” (KAKENHI Grant No. JP20H05154). H. K. was supported by the JSPS through Program for Leading Graduate Schools (ALPS).

- 
- [1] D. Xiao, M.-C. Chang, and Q. Niu, *Rev. Mod. Phys.* **82**, 1959 (2010).
- [2] K. v. Klitzing, G. Dorda, and M. Pepper, *Phys. Rev. Lett.* **45**, 494 (1980).
- [3] D. J. Thouless, M. Kohmoto, M. P. Nightingale, and M. den Nijs, *Phys. Rev. Lett.* **49**, 405 (1982).
- [4] S. Murakami, N. Nagaosa, and S.-C. Zhang, *Science* **301**, 1348 (2003).
- [5] J. Sinova, S. O. Valenzuela, J. Wunderlich, C. H. Back, and T. Jungwirth, *Rev. Mod. Phys.* **87**, 1213 (2015).
- [6] C. L. Kane and E. J. Mele, *Phys. Rev. Lett.* **95**, 226801 (2005).
- [7] C. L. Kane and E. J. Mele, *Phys. Rev. Lett.* **95**, 146802 (2005).
- [8] I. Sodemann and L. Fu, *Phys. Rev. Lett.* **115**, 216806 (2015).
- [9] Z. Z. Du, C. M. Wang, H.-Z. Lu, and X. C. Xie, *Phys. Rev. Lett.* **121**, 266601 (2018).
- [10] R. Battilomo, N. Scopigno, and C. Ortix, *Phys. Rev. Lett.* **123**, 196403 (2019).
- [11] J. Son, K.-H. Kim, Y. H. Ahn, H.-W. Lee, and J. Lee, *Phys. Rev. Lett.* **123**, 036806 (2019).
- [12] J.-S. You, S. Fang, S.-Y. Xu, E. Kaxiras, and T. Low, *Phys. Rev. B* **98**, 121109(R) (2018).
- [13] Y. Zhang, Y. Sun, and B. Yan, *Phys. Rev. B* **97**, 041101(R) (2018).
- [14] S.-Y. Xu, Q. Ma, H. Shen, V. Fatemi, S. Wu, T.-R. Chang, G. Chang, A. M. Mier Valdivia, C.-K. Chan, Q. D. Gibson, J. Zhou, Z. Liu, K. Watanabe, T. Taniguchi, H. Lin, R. J. Cava, L. Fu, N. Gedik, and P. Jarillo-Herrero, *Nat. Phys.* **14**, 900–906 (2018).
- [15] J.-X. Hu, C.-P. Zhang, Y.-M. Xie, and K. T. Law, *arXiv:2004.14140*.
- [16] C.-P. Zhang, J. Xiao, B. T. Zhou, J.-X. Hu, Y.-M. Xie, B. Yan, and K. T. Law, *arXiv:2010.08333*.
- [17] D.-F. Shao, S.-H. Zhang, G. Gurung, W. Yang, and E. Y. Tsymlal, *Phys. Rev. Lett.* **124**, 067203 (2020).
- [18] C. Zeng, S. Nandy, A. Taraphder, and S. Tewari, *Phys. Rev. B* **100**, 245102(2019).
- [19] X.-Q. Yu, Z.-G. Zhu, J.-S. You, T. Low, and G. Su, *Phys. Rev. B* **99**, 201410(R) (2019).
- [20] C. Zeng, S. Nandy, and S. Tewari, *Phys. Rev. Research* **2**, 032066(R) (2020).
- [21] Q. Ma, S.-Y. Xu, H. Shen, D. MacNeill, V. Fatemi, T.-R. Chang, A. M. Mier Valdivia, S. Wu, Z. Du, C.-H. Hsu, S. Fang, Q. D. Gibson, K. Watanabe, T. Taniguchi, R. J. Cava, E. Kaxiras, H.-Z. Lu, H. Lin, L. Fu, N. Gedik, and P. Jarillo-Herrero, *Nature* **565**, 337–342 (2019).
- [22] K. Kang, T. Li, E. Sohn, J. Shan, and K. F. Mak, *Nat. Mater.* **18**, 324–328 (2019).
- [23] Z. Z. Du, H.-Z. Lu, and X. C. Xie, *arXiv:2105.10940*.
- [24] Z. Z. Du, C. M. Wang, H.-P. Sun, H.-Z. Lu, and X. C. Xie, *Nat. Commun.* **12**, 5038 (2021).
- [25] H. Katsura, N. Nagaosa, and P. A. Lee, *Phys. Rev. Lett.* **104**, 066403 (2010).
- [26] R. Matsumoto and S. Murakami, *Phys. Rev. B* **84**, 184406 (2011).
- [27] S. Fujimoto, *Phys. Rev. Lett.* **103**, 047203 (2009).
- [28] R. Shindou, J. I. Ohe, R. Matsumoto, S. Murakami, and E. Saitoh, *Phys. Rev. B* **87**, 174402 (2013).
- [29] R. Shindou, R. Matsumoto, S. Murakami, and J. I. Ohe, *Phys. Rev. B* **87**, 174427 (2013).
- [30] S. K. Kim, H. Ochoa, R. Zarzuela, and Y. Tserkovnyak, *Phys. Rev. Lett.* **117**, 227201 (2016).
- [31] R. Matsumoto, R. Shindou, and S. Murakami, *Phys. Rev. B* **89**, 054420 (2014).
- [32] Y. Onose, T. Ideue, H. Katsura, Y. Shiomi, N. Nagaosa, and Y. Tokura, *Science* **329**, 297 (2010).
- [33] T. Ideue, Y. Onose, H. Katsura, Y. Shiomi, S. Ishiwata, N. Nagaosa, and Y. Tokura, *Phys. Rev. B* **85**, 134411 (2012).
- [34] R. Chisnell, J. S. Helton, D. E. Freedman, D. K. Singh, R. I. Bewley, D. G. Nocera, and Y. S. Lee, *Phys. Rev. Lett.* **115**, 147201 (2015).
- [35] J. H. Han and H. Lee, *J. Phys. Soc. Jpn.* **86**, 011007 (2017).
- [36] S. Murakami and A. Okamoto, *J. Phys. Soc. Jpn.* **86**, 011010 (2017).
- [37] M. Kawano and C. Hotta, *Phys. Rev. B* **99**, 054422 (2019).

- [38] B. Li and A. A. Kovalev, Phys. Rev. B **97**, 174413 (2018).
- [39] M. Hirschberger, R. Chisnell, Y. S. Lee, and N. P. Ong, Phys. Rev. Lett. **115**, 106603 (2015).
- [40] H. Lee, J. H. Han, and P. A. Lee, Phys. Rev. B **91**, 125413 (2015).
- [41] B. Xu, T. Ohtsuki, and R. Shindou, Phys. Rev. B **94**, 220403(R) (2016).
- [42] X. S. Wang, A. Brataas, and R. E. Troncoso, Phys. Rev. Lett. **125**, 217202 (2020).
- [43] Y. Akagi, J. Phys. Soc. Jpn. **89**, 123601 (2020).
- [44] V. A. Zyuzin and A. A. Kovalev, Phys. Rev. Lett. **117**, 217203 (2016).
- [45] K. Nakata, S. K. Kim, J. Klinovaja, and D. Loss, Phys. Rev. B **96**, 224414 (2017).
- [46] A. Mook, R. R. Neumann, J. Henk, and I. Mertig, Phys. Rev. B **100**, 100401(R) (2019).
- [47] H. Kondo, Y. Akagi, and H. Katsura, Phys. Rev. B **99**, 041110(R) (2019).
- [48] H. Kondo, Y. Akagi, and H. Katsura, Phys. Rev. B **100**, 144401 (2019).
- [49] H. Kondo and Y. Akagi, Phys. Rev. Lett. **127**, 177201 (2021).
- [50] S. S. Pershoguba, S. Banerjee, J. C. Lashley, J. Park, H. Ågren, G. Aeppli, and A. V. Balatsky, Phys. Rev. X **8**, 011010 (2018).
- [51] K. Li, C. Li, J. Hu, Y. Li, and C. Fang, Phys. Rev. Lett. **119**, 247202 (2017).
- [52] S. Bao, J. Wang, W. Wang, Z. Cai, S. Li, Z. Ma, D. Wang, K. Ran, Z.-Y. Dong, D. L. Abernathy, S.-L. Yu, X. Wan, J.-X. Li, and J. Wen, Nat. comm. **9**, 2591 (2018).
- [53] J. Fransson, A. M. Black-Schaffer, and A. V. Balatsky, Phys. Rev. B **94**, 075401 (2016).
- [54] F.-Y. Li, Y.-D. Li, Y. B. Kim, L. Balents, Y. Yu, and G. Chen, Nat. comm. **7**, 12691 (2016).
- [55] A. Mook, J. Henk, and I. Mertig, Phys. Rev. Lett. **117**, 157204 (2016).
- [56] S. A. Owerre, J. Phys. Commun. **1**, 025007 (2017).
- [57] Y. Su, X. S. Wang, and X. R. Wang, Phys. Rev. B **95**, 224403 (2017).
- [58] T. Liu and Z. Shi, Phys. Rev. B **99**, 214413 (2019).
- [59] R. Cheng, S. Okamoto, and D. Xiao, Phys. Rev. Lett. **117**, 217202 (2016).
- [60] Y. Shiomi, R. Takashima, and E. Saitoh, Phys. Rev. B **96**, 134425 (2017).
- [61] S. Maekawa, S. O. Valenzuela, E. Saitoh, and T. Kimura, *Spin Current*, (Oxford Univ. Press, 2012).
- [62] A. V. Chumak, V. I. Vasyuchka, and A. A. Serga, Nat. Phys. **11**, 453 (2015).
- [63] A. Mook, B. Göbel, J. Henk, and I. Mertig, Phys. Rev. B **97**, 140401(R) (2018).
- [64] R. Takashima, Y. Shiomi, and Y. Motome, Phys. Rev. B **98**, 020401(R) (2018).
- [65] I. Proskurin, A. S. Ovchinnikov, J. I. Kishine, and R. L. Stamps, Phys. Rev. B **98**, 134422 (2018).
- [66] H. Ishizuka and M. Sato, Phys. Rev. B **100**, 224411 (2019).
- [67] C. Cercignani, *The Boltzmann Equation and Its Applications*. Springer, New York (1988).
- [68] J. Callaway, *Quantum Theory of the Solid State*. Academic Press, London (1974).
- [69] G. D. Mahan, *Many-Particle Physics*, 3rd. Edition (2000).
- [70] See Supplemental Material at [URL for Supplemental Material] for detailed calculations.
- [71] H. Kondo, Y. Akagi, and H. Katsura, Prog. Theor. Exp. Phys. **2020**, 12A104 (2020).
- [72] It can also be understood from BC and band structure which are antisymmetric and symmetric about  $\Gamma$  point, respectively, as shown in Figs. 3(a)-(d).
- [73] A. R. Wildes, B. Roessli, B. Lebech, and K. W. Godfrey, J. Phys.: Condens. Matter **10** 6417 (1998).
- [74] D. Hirobe, M. Sato, T. Kawamata, Y. Shiomi, K. Uchida, R. Iguchi, Y. Koike, S. Maekawa, and E. Saitoh, Nat. Phys. **13**, 30 (2017).
- [75] One can easily make sure that these AFMs also have  $\mathcal{PT}$ -symmetry thanks to the same form of the magnon Hamiltonian as that expressed in Eq. (7).
- [76] The systems without inversion symmetry can possess the DMI and thus have the potential for exhibiting the linear SNE. However, if materials consist of light elements, they can show mainly not the linear but nonlinear SNE because the strain-induced DMI would be negligible.
- [77] C. I. Hiley, M. R. Lees, J. M. Fisher, D. Thompson, S. Agrestini, R. I. Smith, and R. I. Walton, Angew. Chem. Int. Ed. **53**, 4423 (2014).
- [78] Y. S. Ponosov, E.V. Komleva, D.A. Zamyatin, R. I. Walton, and S.V. Streltsov, Phys. Rev. B **99**, 085103 (2019).
- [79] T. Okabe, H. Yamaguchi, S. Kittaka, T. Sakakibara, T. Ono, and Y. Hosokoshi, Phys. Rev. B **95**, 075120 (2017).
- [80] G. Sala, M. B. Stone, B. K. Rai, A. F. May, P. Laurell, V. O. Garlea, N. P. Butch, M. D. Lumsden, G. Ehlers, G. Pokharel, A. Podlesnyak, D. Mandrus, D. S. Parker, S. Okamoto, G. D. Halasz, and A. D. Christianson, Nat. Commun. **12**, 171 (2021).
- [81] I. Spremo, F. Schütz, P. Kopietz, V. Pashchenko, B. Wolf, M. Lang, J. W. Bats, C. Hu, and M. U. Schmidt, Phys. Rev. B **72**, 174429 (2005).
- [82] A. A. Tsirlin, O. Janson, and H. Rosner, Phys. Rev. B **82**, 144416 (2010).
- [83] M. Yehia, E. Vavilova, A. Möller, T. Taetz, U. Löw, R. Klingeler, V. Kataev, and B. Büchner, Phys. Rev. B **81**, 060414(R) (2010).
- [84] L. Lederová, A. Orendáčová, J. Chovan, J. Strečka, T. Verkholyak, R. Tarasenko, D. Legut, R. Sýkora, E. Čížmár, V. Tkáč, M. Orendáč, and A. Feher, Phys. Rev. B **95**, 054436 (2017).
- [85] L. Ge, J. Flynn, J. A. M. Paddison, M. B. Stone, S. Calder, M. A. Subramanian, A. P. Ramirez, and M. Mourigal, Phys. Rev. B **96**, 064413 (2017).
- [86] A. Krimmel, H. Mutka, M. M. Koza, V. Tsurkan, and A. Loidl, Phys. Rev. B **79**, 134406 (2009).
- [87] Y. Shimizu, A. Otsuka, M. Maesato, M. Tsuchiizu, A. Nakao, H. Yamochi, T. Hiramatsu, Y. Yoshida, and G. Saito, Phys. Rev. B **99**, 174417 (2019).
- [88] M. Naka, S. Hayami, H. Kusunose, Y. Yanagi, Y. Motome, and H. Seo, Nat. Commun. **10**, 4305 (2019).
- [89] M. Naka, S. Hayami, H. Kusunose, Y. Yanagi, Y. Motome, and H. Seo, Phys. Rev. B **102**, 075112 (2020).

### Derivation of the nonlinear transverse current of magnons

In this part, we provide a detailed derivation of the formula for the nonlinear transverse current of magnons expressed as Eq. (3) in the main text by solving the Boltzmann equation. The Boltzmann equation in the relaxation time approximation [67–69] is written as follows:

$$\begin{aligned} & \frac{\partial}{\partial t} \rho(E_n(\mathbf{k}) + \epsilon, T(x)) + \dot{r}_i \frac{\partial}{\partial r_i} \rho(E_n(\mathbf{k}) + \epsilon, T(x)) + \dot{k}_i \frac{\partial}{\partial k_i} \rho(E_n(\mathbf{k}) + \epsilon, T(x)) \\ &= - \frac{\rho(E_n(\mathbf{k}) + \epsilon, T(x)) - \rho_0(E_n(\mathbf{k}) + \epsilon, T(x))}{\tau}, \end{aligned} \quad (\text{S.1})$$

On the left-hand side of Eq. (S.1), the first and third terms vanish because we assume the steady-state and the system without external field. Thus, the Boltzmann equation Eq. (S.1) can be rewritten as Eq. (2) in the main text, i.e.,

$$\dot{x} \frac{\partial}{\partial x} \rho(E_n(\mathbf{k}) + \epsilon, T(x)) = - \frac{\rho(E_n(\mathbf{k}) + \epsilon, T(x)) - \rho_0(E_n(\mathbf{k}) + \epsilon, T(x))}{\tau}. \quad (\text{S.2})$$

Next, we solve Eq. (S.2) up to the first order in  $\nabla T$ . We deform Eq. (S.2) as follows:

$$\begin{aligned} \rho(E_n(\mathbf{k}) + \epsilon, T(x)) &= \rho_0(E_n(\mathbf{k}) + \epsilon, T(x)) - \tau \dot{x} \frac{\partial}{\partial x} \rho_0(E_n(\mathbf{k}) + \epsilon, T(x)) + O((\nabla T)^2) \\ &= \rho_0(E_n(\mathbf{k}) + \epsilon, T(x)) - \frac{\tau}{\hbar} \frac{\partial E_n(\mathbf{k})}{\partial k_x} \frac{\partial}{\partial x} \rho_0(E_n(\mathbf{k}) + \epsilon, T(x)) + O((\nabla T)^2). \end{aligned} \quad (\text{S.3})$$

Let us calculate the  $x$ -derivative of  $\rho(\epsilon, T(x))$  which appears in Eq. (1) in the main text:

$$\begin{aligned} \frac{\partial}{\partial x} \rho(E_n(\mathbf{k}) + \epsilon, T(x)) &= \frac{\partial}{\partial x} \rho_0(E_n(\mathbf{k}) + \epsilon, T(x)) - \frac{\tau}{\hbar} \frac{\partial E_n(\mathbf{k})}{\partial k_x} \frac{\partial^2}{\partial x^2} \rho_0(E_n(\mathbf{k}) + \epsilon, T(x)) + O((\nabla T)^3) \\ &= -\nabla T \frac{\partial}{\partial T_0} \rho_0(E_n(\mathbf{k}) + \epsilon, T_0) + x(\nabla T)^2 \frac{\partial^2}{\partial T_0^2} \rho_0(E_n(\mathbf{k}) + \epsilon, T_0) \\ &\quad - \frac{\tau}{\hbar} (\nabla T)^2 \frac{\partial E_n(\mathbf{k})}{\partial k_x} \frac{\partial^2}{\partial T_0^2} \rho_0(E_n(\mathbf{k}) + \epsilon, T_0) + O((\nabla T)^3). \end{aligned} \quad (\text{S.4})$$

The second term in the final expression vanishes in the whole space since it is an odd function of  $x$ . Thus, by substituting Eq. (S.4) to Eq. (1) in the main text, we obtain the expression of the transverse magnon current as up to a second-order response to the temperature gradient  $\nabla T$ :

$$J_y = \frac{\nabla T}{\hbar V} \sum_{n, \mathbf{k}} \Omega_n(\mathbf{k}) \frac{\partial}{\partial T_0} \int_0^\infty d\epsilon \rho_0(E_n(\mathbf{k}) + \epsilon, T_0) + \frac{\tau (\nabla T)^2}{\hbar^2 V} \sum_{n, \mathbf{k}} \Omega_n(\mathbf{k}) \frac{\partial E_n(\mathbf{k})}{\partial k_x} \frac{\partial^2}{\partial T_0^2} \int_0^\infty d\epsilon \rho_0(E_n(\mathbf{k}) + \epsilon, T_0) + O((\nabla T)^3). \quad (\text{S.5})$$

We note that the following equation holds:

$$\frac{\partial}{\partial T_0} \int_0^\infty d\epsilon \rho_0(E_n(\mathbf{k}) + \epsilon, T_0) = c_1(\rho_0(E_n(\mathbf{k}), T_0)), \quad (\text{S.6})$$

where the function  $c_1(\rho_0)$  is defined as  $c_1(\rho_0) := (1 + \rho_0) \ln(1 + \rho_0) - \rho_0 \ln \rho_0$ . By using Eq. (S.6) and replacing the sum over  $\mathbf{k}$  with the integral, the second term in the right-hand side of Eq. (S.5) can be rewritten as follows:

$$\begin{aligned} \sum_{n, \mathbf{k}} \Omega_n(\mathbf{k}) \frac{\partial E_n(\mathbf{k})}{\partial k_x} \frac{\partial^2}{\partial T_0^2} \int_0^\infty d\epsilon \rho_0(E_n(\mathbf{k}) + \epsilon, T_0) &= \sum_{n, \mathbf{k}} \Omega_n(\mathbf{k}) \frac{\partial E_n(\mathbf{k})}{\partial k_x} \frac{\partial}{\partial T_0} c_1(\rho_0(E_n(\mathbf{k}), T_0)) \\ &= \sum_n \int_{\text{BZ}} d^2 k \Omega_n(\mathbf{k}) \frac{\partial E_n(\mathbf{k})}{\partial k_x} \left( - \frac{E_n(\mathbf{k})}{T_0} \right) \frac{\partial}{\partial E_n(\mathbf{k})} c_1(\rho_0(E_n(\mathbf{k}), T_0)) \\ &= - \frac{1}{T_0} \sum_n \int_{\text{BZ}} d^2 k E_n(\mathbf{k}) \Omega_n(\mathbf{k}) \frac{\partial}{\partial k_x} c_1(\rho_0(E_n(\mathbf{k}), T_0)) \\ &= \frac{1}{T_0} \sum_n \int_{\text{BZ}} d^2 k c_1(\rho_0(E_n(\mathbf{k}), T_0)) \frac{\partial}{\partial k_x} (E_n(\mathbf{k}) \Omega_n(\mathbf{k})). \end{aligned} \quad (\text{S.7})$$

Since the function  $c_1(\rho_0(E_n(\mathbf{k}), T_0))$  depends on  $T_0$  via the distribution function  $\rho_0(E_n(\mathbf{k}), T_0) = [e^{E_n(\mathbf{k})/T_0} - 1]^{-1}$ , the  $T_0$ -derivative can be replaced with  $(-E_n(\mathbf{k})/T_0)\partial/\partial E_n(\mathbf{k})$ . We used it in the second equality in Eqs. (S.7). Eventually, the transverse magnon current up to the second-order of the temperature gradient  $\nabla T$  in Eq. (S.5) can be written as Eq. (3) in the main text, i.e.,

$$J_y = \frac{\nabla T}{\hbar V} \sum_n \int_{\text{BZ}} d^2k c_1(\rho_0(E_n(\mathbf{k}), T_0)) \Omega_n(\mathbf{k}) + \frac{\tau(\nabla T)^2}{\hbar^2 V T_0} \sum_n \int_{\text{BZ}} d^2k c_1(\rho_0(E_n(\mathbf{k}), T_0)) \frac{\partial}{\partial k_x} (E_n(\mathbf{k}) \Omega_n(\mathbf{k})) + O((\nabla T)^3). \quad (\text{S.8})$$

### Order estimation of nonlinear spin Nernst current

In the main text, we discuss the order of the nonlinear SNE by comparing the linear ones observed in the honeycomb antiferromagnet MnPS<sub>3</sub> [60]. In this part, we give the details for the order estimation. To begin with, we discuss the linear SNE in MnPS<sub>3</sub> with the DMI. We here consider the following Hamiltonian for the antiferromagnet MnPS<sub>3</sub>:

$$\mathcal{H} = J_1 \sum_{\langle ij \rangle_1} \mathbf{S}_i \cdot \mathbf{S}_j + J_2 \sum_{\langle ij \rangle_2} \mathbf{S}_i \cdot \mathbf{S}_j + D \sum_{\langle\langle ij \rangle\rangle} \xi_{ij} (\mathbf{S}_i \times \mathbf{S}_j)_z - \kappa \sum_i (S_i^z)^2, \quad (\text{S.9})$$

where the third term is the DMI between the second nearest neighbor spins. The sign convention of the DMI  $\xi_{ij}$  is shown in Fig. S1. Other terms are the same as those in model (6) in the main text. By applying Holstein-Primakoff and Fourier transformations, we obtain the magnon Hamiltonian for model (S.9), which is written as in the same form as in Eq. (7) with the additional term  $\Delta(\mathbf{k})$  derived from the DMI, i.e.,

$$H(\mathbf{k}) = \begin{pmatrix} d - \Delta(\mathbf{k}) & 0 & 0 & \gamma(\mathbf{k}) \\ 0 & d + \Delta(\mathbf{k}) & \gamma^*(\mathbf{k}) & 0 \\ 0 & \gamma(\mathbf{k}) & d + \Delta(\mathbf{k}) & 0 \\ \gamma^*(\mathbf{k}) & 0 & 0 & d - \Delta(\mathbf{k}) \end{pmatrix}, \quad (\text{S.10})$$

$$\Delta(\mathbf{k}) = 2DS \left[ \sin \left( -\frac{1}{2}k_x + \frac{\sqrt{3}}{2}k_y \right) - \sin \left( \frac{1}{2}k_x + \frac{\sqrt{3}}{2}k_y \right) + \sin(k_x) \right]. \quad (\text{S.11})$$

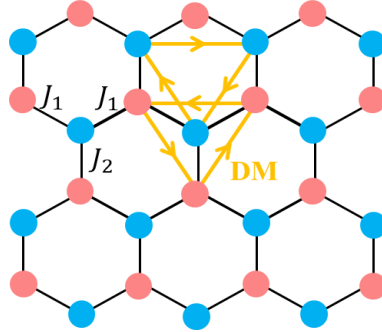


FIG. S1: Honeycomb lattice corresponding to the antiferromagnet MnPS<sub>3</sub>. The sign convention  $\xi_{ij} = +1$  ( $= -\xi_{ji}$ ) for  $i \rightarrow j$  is indicated by the orange arrows.

The experiment [60] shows a good agreement with the theoretical study [59], in which the parameters of MnPS<sub>3</sub> are considered as  $J_1 = J_2 = 1.54$  meV,  $D = 0.36$  meV,  $\kappa S = 0.0086$  meV, and  $S = 5/2$ . To estimate the order of linear spin Nernst current, we ignore the second and the third nearest neighbor Heisenberg interactions taken into account in Ref. [59], whose coupling constants are less than one-fourth of the nearest neighbor ones. Since the antiferromagnet MnPS<sub>3</sub> possesses the nonnegligible DMI, the spin current observed in MnPS<sub>3</sub> [60] is mainly attributed to the linear SNE, which is described by the first term in Eq. (5) in the main text. Here, we write the part of the integral in this term as follows:

$$I_1 := \sum_n \int_{\text{BZ}} d^2k c_1(\rho_0(E_n(\mathbf{k}), T_0)) (\Omega_{n,\uparrow}(\mathbf{k}) - \Omega_{n,\downarrow}(\mathbf{k})). \quad (\text{S.12})$$

Figure S2(a) shows the numerical result of  $I_1$  as a function of temperature  $T_0$  in model (S.9). From the figure, the

order of the spin current at  $T_0 = 20$  K can be written as follows:

$$J_L^S = \frac{\nabla T}{V} \times I_1 \sim \frac{\nabla T}{V} \times 10^{-1}. \quad (\text{S.13})$$

Next, we estimate the order of nonlinear SNE in model (S.9) where the DMI is set to be zero, which is equivalent to model (6) in the main text. We here assume that the coupling constant  $J_1$  in Eq. (6) is changed as  $J_1 = 1.54 \rightarrow 2.0$  meV. In such a case, i.e., for  $D = 0$  and  $J_1 \neq J_2$ , the model does not exhibit the linear magnon SNE, but the nonlinear one, which is described by the second term in Eq. (5) in the main text. Here, we write the part of the integral of this term with the prefactor  $1/T_0$  as  $I_2$ , i.e.,

$$I_2 := \frac{1}{T_0} \sum_n \int_{\text{BZ}} d^2k c_1(\rho_0(E_n(\mathbf{k}), T_0)) \frac{\partial}{\partial k_x} [E_n(\mathbf{k}) (\Omega_{n,\uparrow}(\mathbf{k}) - \Omega_{n,\downarrow}(\mathbf{k}))]. \quad (\text{S.14})$$

The numerical result of  $I_2$  as a function of  $T_0$  is shown in Fig. S2(b). From this figure, we can evaluate the nonlinear spin current at  $T_0 = 20$  K as

$$J_{NL}^S = \frac{\tau(\nabla T)^2}{\hbar V} \times I_2 \sim \frac{\tau(\nabla T)^2}{\hbar V} \times (10^{-1} \text{ meV} \cdot \text{nm} \cdot \text{K}^{-1}). \quad (\text{S.15})$$

Since the linear spin Nernst current in Eq. (S.13) was observed with the electric voltage  $V_L \sim 1 \mu\text{V}$  through the inverse spin Hall effect at  $T_0 = 20$  K (see Fig. 3(c) in Ref. [60]), we can estimate the voltage  $V_{NL}$  by the nonlinear spin Nernst current in Eq. (S.15) in the following by taking their ratio:

$$\begin{aligned} V_{NL} &\sim V_L \times \frac{J_{NL}^S}{J_L^S} \\ &\sim 1 \mu\text{V} \times \frac{(\tau(\nabla T)^2/\hbar V) \times (10^{-1} \text{ meV} \cdot \text{nm} \cdot \text{K}^{-1})}{(\nabla T/V) \times 10^0} \\ &\sim 10^{n+6} \mu\text{V}. \end{aligned} \quad (\text{S.16})$$

Here, we assume that the lifetime of magnons and the applied temperature gradient are  $\tau \sim 10^n$  s and  $\nabla T \sim 10^{-6}$  K · nm<sup>-1</sup>, respectively. In experiments, the minimum voltage detectable through the inverse Hall effect is roughly  $10^{-3} \mu\text{V}$  [74], and thus we can detect the nonlinear SNE if the magnon lifetime is  $\tau \gtrsim 1$  ns. In model (6), the velocity of magnons is estimated as  $v = (\partial/\hbar \partial k_i) E_{\uparrow}(\mathbf{k}) \sim 10^{12}$  nm · s<sup>-1</sup>. Then, the corresponding mean free path for  $V_{NL} \sim 10^{-3} \mu\text{V}$  ( $\tau \sim 1$  ns) is  $l \sim 1 \mu\text{m}$ , which is achievable in magnets.

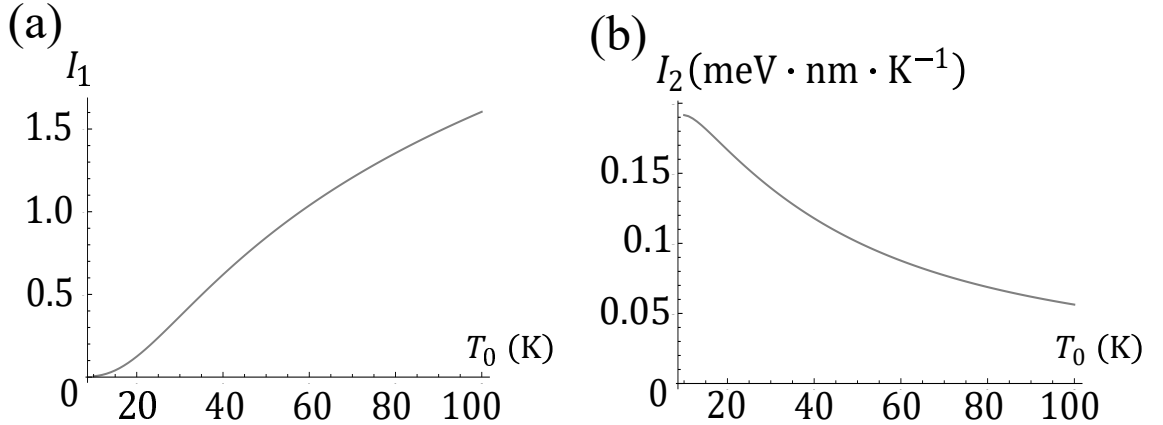


FIG. S2: Numerical results of (a)  $I_1$  and (b)  $I_2$  defined as Eqs. (S.12) and (S.14), respectively. The parameters  $J_1$  and  $D$  are chosen to be (a)  $J_1 = 1.54$  meV and  $D = 0.36$  meV, and (b)  $J_1 = 2.0$  meV and  $D = 0$ , respectively. In both (a) and (b), the other parameters  $J_2$ ,  $\kappa$ , and  $S$  are taken as  $J_2 = 1.54$  meV,  $\kappa S = 0.0086$  meV, and  $S = 5/2$ , respectively. We note that  $I_1$  is dimensionless. In particular, at the temperature  $T_0 = 20$  K, the orders of them are  $I_1 \sim 10^{-1}$  and  $I_2 \sim 10^{-1}$  meV · nm · K<sup>-1</sup>, respectively.

In the main text, we discussed BC and BCD of magnons in the square and diamond lattice AFMs illustrated as Fig. 4. In this section, we give the explicit expressions of magnon Hamiltonians for these systems, which can be obtained by applying Holstein-Primakoff and Fourier transformations to Eq. (6) in the main text. The magnon Hamiltonian of these AFMs can be written in the same form as Eq. (7). In the case of the square lattice AFMs with staggered-bond dependence [see Fig. 4(a)],  $d$  and  $\gamma(\mathbf{k})$  in Eq. (7) is defined as follows:

$$d = 3J_1S + J_2S + 2\kappa S, \quad (\text{S.17})$$

$$\gamma(\mathbf{k}) = J_1S e^{ik_x/\sqrt{2}} + J_1S e^{ik_y/\sqrt{2}} + J_2S e^{-ik_x/\sqrt{2}} + J_1S e^{-ik_y/\sqrt{2}}. \quad (\text{S.18})$$

Those of the square lattice AFMs with zigzag-bond dependence [see Fig. 4(b)] are given by

$$d = 2J_1S + 2J_2S + 2\kappa S, \quad (\text{S.19})$$

$$\gamma(\mathbf{k}) = J_1S e^{ik_x/\sqrt{2}} + J_1S e^{ik_y/\sqrt{2}} + J_2S e^{-ik_x/\sqrt{2}} + J_2S e^{-ik_y/\sqrt{2}}. \quad (\text{S.20})$$

In the case of diamond lattice AFM [see Fig. 4(c)],  $d$  and  $\gamma(\mathbf{k})$  are written as follows:

$$d = 3J_1S + J_2S + 2\kappa S, \quad (\text{S.21})$$

$$\gamma(\mathbf{k}) = J_1S e^{i\mathbf{k}\cdot\mathbf{a}_0} + J_1S e^{i\mathbf{k}\cdot\mathbf{a}_1} + J_1S e^{i\mathbf{k}\cdot\mathbf{a}_2} + J_2S e^{i\mathbf{k}\cdot\mathbf{a}_3}, \quad (\text{S.22})$$

where  $\mathbf{a}_0 = \left(0, \frac{1}{\sqrt{3}}, -\frac{1}{2\sqrt{6}}\right)$ ,  $\mathbf{a}_1 = \left(-\frac{1}{2}, -\frac{1}{2\sqrt{3}}, -\frac{1}{2\sqrt{6}}\right)$ ,  $\mathbf{a}_2 = \left(\frac{1}{2}, -\frac{1}{2\sqrt{3}}, -\frac{1}{2\sqrt{6}}\right)$ , and  $\mathbf{a}_3 = \left(0, 0, \frac{3}{4}\sqrt{\frac{2}{3}}\right)$ .

### Nonlinear magnon spin Nernst current in various antiferromagnets

In this part, we show the numerical results of the nonlinear magnon spin Nernst current in the AFMs illustrated as Fig. 4. Figure S3 shows the coefficients of nonlinear magnon SNE in these systems as a function of the coupling constant  $J_2$ . For the case of the diamond lattice AFM, we generalize the formula Eq. (5) in the main text to that in three dimensions; i.e.,

$$\begin{aligned} J_z^S &= \frac{\nabla T}{V} \sum_n \int_{\text{BZ}} d^3k c_1(\rho_0(E_n(\mathbf{k}), T_0)) (\Omega_{n,\uparrow}^x(\mathbf{k}) - \Omega_{n,\downarrow}^x(\mathbf{k})) \\ &+ \frac{\tau(\nabla T)^2}{\hbar V T_0} \sum_n \int_{\text{BZ}} d^3k c_1(\rho_0(E_n(\mathbf{k}), T_0)) \frac{\partial}{\partial k_y} (E_n(\mathbf{k}) (\Omega_{n,\uparrow}^x(\mathbf{k}) - \Omega_{n,\downarrow}^x(\mathbf{k}))) \\ &+ O((\nabla T)^3). \end{aligned} \quad (\text{S.23})$$

From Fig. S3, we can see that the nonlinear SNE of magnons occurs in the square and diamond lattice AFMs. In particular, Fig. S3(c) implies that the pressure-tunable spin current can generate in the diamond lattice AFM as well as the honeycomb lattice AFM.

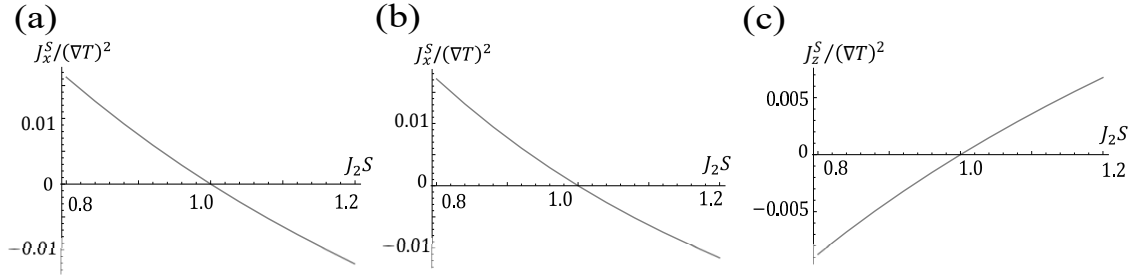


FIG. S3: Coefficients of nonlinear magnon SNE in the square lattice AFMs with the (a) staggered-, (b) zigzag-bond dependences, and (c) the diamond lattice AFM under pressure. The temperature gradient is applied in the  $y$ -direction as  $T(y) = T_0 - y\nabla T$ . In the case of diamond lattice AFM, the spin Nernst current flows to the  $+z$ -direction ( $-z$ -direction) for  $J_1 < J_2$  ( $J_1 > J_2$ ). We set  $J_1S = 1.0$ ,  $\kappa S = 0.01$ ,  $T_0 = 0.1$  and take the factor  $\tau/(\hbar V T_0) = 1$  for (a), (b), and (c).